THE PHYSICS OF FLUIDS VOLUME 15, NUMBER 6 JUNE 1972

End Effect in Langmuir Probe Response under Ionospheric Satellite Conditions

JUAN R. SANMARTIN*
Department of Mechanical Engineering Massachusetts Institute of Technology, Cambridge, Massachusetts 02139
(Received 8 April 1971; Final manuscript received 17 November 1971)

A theory is presented for an end effect in the current response of a highly negative, cylindrical Langmuir probe in a collisionless plasma flow. Under conditions where the ratio of probe radius to Debye length is small and the ion-acoustic Mach number is large, the current exhibits a strong peak when the probe axis is brought into alignment with the flow direction. Closed formulas are given for the maximum and angular half-width of the peak, and universal graphical results are presented for the entire peak structure. The theory shows very good agreement with experimental data. The use of the end effect for diagnostic purposes, in particular, for the determination of the ion temperature, is discussed.

I. INTRODUCTION

The theory of an infinitely long, cylindrical Langmuir probe in a collisionless, quiescent plasma is particularly simple when the probe radius r_p is smaller than the Debye length λ_D, since then the current is "orbital motion limited"[1] and the old Langmuir analysis[2] is valid. The analysis is approximately valid even in the more general case in which the plasma is in motion relative to the probe.[2] If θ is the angle between probe axis and flow direction, and $-eV_p$ and $m_iU^2 \gg \kappa T_e$, κT_i (where V_p is the applied potential, κT_e is the electron thermal energy and κT_i and $m_iU^2/2$ are the ion thermal and directed energies, respectively) the current J_∞ to a probe of length l, as $l \to \infty$, is given by[2]

$$J_\infty/l \approx 2N_0eU \sin\theta\, r_p[1-2Z_ieV_p/m_iU^2 \sin^2\theta]^{1/2}, \quad (1)$$

where N_0 is the plasma density and Z_i is the ion charge number. Notice that according to Eq. (1) J_∞ decreases monotonically as θ goes from $\frac{1}{2}\pi$ to zero.

In any actual experiment, however, l must be finite. Recently, (ion attracting probe) current data have been reported from both satellite[3] and laboratory[4] experiments, for $r_p \ll \lambda_D$, $m_iU^2 \gg Z_i\kappa T_e$, and l/r_p as high as 820, that show a striking disagreement with J_∞ as given in Eq. (1). The current observed J was close to J_∞ as long as θ was not small, but as the probe approached the aligned orientation J exhibited a sharp rise that peaked at $\theta=0$ at a value many times larger than $J_\infty(\theta=0)$. This phenomenon may be explained[3,5] as an end effect due to the finite length of the probe. This shows that extremely long probes may be necessary if Eq. (1) is to be applicable in the interpretation of probe characteristics.

Of more interest for diagnostic purposes, however, is the end effect in itself. The peak may be quite strong, and it should be possible to use it in the determination of the relative direction of the plasma flow, and of a number of plasma parameters. Of particular interest is the fact that both the height and the half-width of the peak are often sensitive to the ion temperature. This is very important because no other feature of probe response is known to be noticeably dependent on T_i.

Bettinger and Chen[3] were the first authors to present a theoretical, although rough, analysis of the end effect; an important limitation of their approach, as pointed out in Ref. 5, was that l had to exceed a minimum value l_m [$l_m \approx 3\lambda_D(m_iU^2/Z_i\kappa T_e)^{1/2}$]. For $l \gtrsim l_m$ some numerical computations were carried out by Hester and Sonin[5] for $\theta=0$.

The present analysis is valid for $\lambda_D \ll l \gtrsim l_m$ and θ arbitrary within the peak region, and starts from a similarity, suggested in Ref. 5, between the present steady-flow problem and a time-dependent one involving a quiescent plasma. In the next section, the basic points of a theory[6] recently developed for the time-dependent problem are introduced. In Sec. III analytical and graphical results for the main features of the end effect are presented and compared with experimental data. The applications of the effect are discussed in Sec. IV, and Bettinger and Chen's analysis is discussed in an Appendix.

Our analysis is based on a number of approximations. Obviously justifiable are the use of Boltzmann's law for the electron density, and the neglect of ion thermal motion in the direction of the probe axis (Sec. II). The validity of the Hester–Sonin similarity rests upon several simplifications: (1) the ion velocity along the probe axis is approximated by the unperturbed value U; the second derivatives of the potential (2) along the probe axis, and (3) with respect to an azimuthal angle around that axis, are neglected in Poisson's equation; (4) the field ahead of the probe tip, and (5) the change in ion angular momentum, are also neglected. Approximations (1) and (2) are justified in Sec. II, and approximations (3), (4), and (5), in the Appendix. The solution of the time-dependent model problem itself is obtained by approximating the potential field in a given neighborhood of the probe by a certain time-independent field (Sec. II).

II. BASIC FORMULATION

We consider a long, cylindrical Langmuir probe with length l and radius r_p in a collisionless plasma with unperturbed thermal energies κT_e and κT_i, density N_0 and bulk velocity relative to the probe U at an angle θ

with its axis. The probe potential V_p is negative such that

$$m_e U^2 \ll \kappa T_e \ll -eV_p; \tag{2}$$

the electron current is then negligible and the perturbed electron density is given by Boltzmann's law

$$N_e = N_0 \exp(-\psi), \tag{3}$$

where $\psi \equiv -eV/\kappa T_e$ is the nondimensional potential field. Defining

$$\beta = T_i/Z_i T_e, \qquad M = U/\lambda_D \omega_{pi}, \tag{4}$$

$$\hat{l} = l/\lambda_D, \qquad \epsilon = r_p/\lambda_D, \tag{5}$$

we assume that M and $\hat{l}$ are large, ϵ is small and $\beta \leq 1$; M is the ion-acoustic Mach number, $\lambda_D \equiv (\kappa T_e/4\pi N_0 e^2)^{1/2}$ is the electron Debye length, $\omega_{pi} \equiv (4\pi N_0 Z_i e^2/m_i)^{1/2}$ is the ion plasma frequency and m_i and Z_i are the ion mass and charge number. If $j(z)$ is the current density at the probe at distance z from its tip,[7] the average current density

$$\bar{j} = l^{-1} \int_0^l j(z)\, dz$$

can then be written as a nondimensional function

$$\bar{j}/j_\infty = (\bar{j}/j_\infty)(\hat{l}, M, \epsilon, \beta, \psi_p, \theta), \tag{6}$$

where $j_\infty \equiv \bar{j}(\hat{l} \to \infty)$; according to Eq. (1)

$$j_\infty \approx \pi^{-1} N_0 eU \sin\theta [1 - 2Z_i eV_p/m_i U^2 \sin^2\theta]^{1/2}. \tag{7}$$

The total current to the probe is $J = 2\pi r_p l j_\infty$ times $\bar{j}/j_\infty$. To obtain this last quantity, the ion Vlasov equation must be solved together with Eq. (3) and Poisson's equation. The last one is

$$\rho^{-1} \frac{\partial}{\partial \rho} \rho \frac{\partial \psi}{\partial \rho} + \frac{1}{\rho^2} \frac{\partial^2 \psi}{\partial \phi^2} + \frac{\epsilon^2}{\hat{l}^2} \frac{\partial^2 \psi}{\partial \zeta^2} = \epsilon^2 \nu; \tag{8}$$

we have introduced cylindrical coordinates r, ϕ, and z and have defined dimensionless quantities

$$\rho = r/r_p, \qquad \zeta = z/l, \qquad \nu_i = (Z_i N_i - N_e)/N_0, \tag{9}$$

where N_i is the perturbed ion density. ψ equals $\psi_p \equiv -eV_p/\kappa T_e$, at the probe and zero at infinity. The ion distribution function far ahead of the probe must also be known [even though $U \gg (\kappa T_i/m_i)^{1/2}$] and here will be assumed to be Maxwellian. [Thermal velocities may, and will, be neglected in the motion along the z axis, but thermal motion in the (ρ, ϕ) plane is of fundamental importance when θ is small.] The probe surface is assumed to be perfectly absorbing.

Let us begin by considering the limit $\theta = 0$ (which also implies $\partial/\partial\phi = 0$). Hester and Sonin[5] studied this limit and pointed out that, if $\hat{l}$ and M^2/ψ_p are so large that $\partial^2\psi/\partial\zeta^2$ can be neglected in Eq. (8) and the ion velocity along the z axis can be well approximated by its unperturbed value U, the steady-flow problem

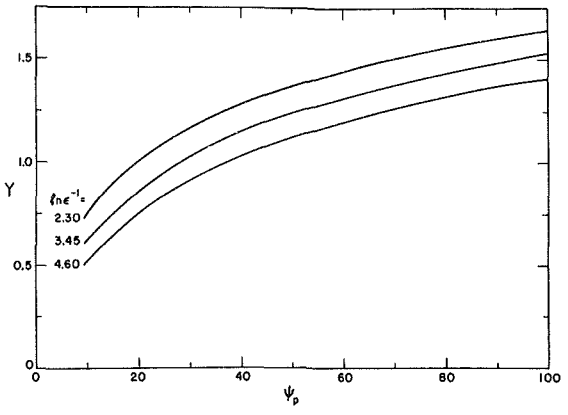

FIG. 1. Potential field parameter Y, introduced in Eq. (15), versus nondimensional probe potential ψ_p and nondimensional probe radius ϵ (defined in first paragraph of Sec. II).

is equivalent to a time-dependent one, wherein an infinitely long probe is immersed at time $t = 0$ in an unperturbed quiescent plasma, all other conditions being the same as those of the original problem. The time of flight of the ions down the probe z/U and the current density at z are, respectively, equivalent to the time t and the (spatially uniform) current density at t. As $z(t)$ increases, the ion distribution function readjusts itself and, if l is large enough, the "infinite" probe (steady state) limiting current density $j_\infty(\theta = 0)$ will eventually be reached. In the context of the time-dependent problem we can write

$$\frac{\bar{j}}{j_\infty}(\theta = 0) = t_l^{-1} \int_0^{t_l} \frac{j(t)}{j_\infty(\theta = 0)}\, dt, \tag{10}$$

where

$$t_l = l/U \tag{11}$$

is the time equivalent of the length of the probe in the flowing plasma.

The time-dependent problem has recently been analyzed by Sanmartin.[6] His approach is based on the following points: (i) It is possible to derive an accurate expression for the electric field $\partial\psi/\partial\rho$ (for limited values of ρ) without simultaneously solving the ion Vlasov equation. Integrating Poisson's equation

$$\rho^{-1} \frac{\partial}{\partial \rho} \rho \frac{\partial \psi}{\partial \rho} = \epsilon^2 \nu \tag{12}$$

yields a formal expression

$$\frac{\partial \psi}{\partial \rho} = -\frac{\psi_p \delta(t)}{\rho} + \frac{\epsilon^2}{2\rho} (\rho^2 - 1) \langle \nu(\rho, t) \rangle, \tag{13}$$

where $-\psi_p \delta(t)$ is the field at the probe at time t and $\langle \nu \rangle$ is defined by

$$(\rho^2 - 1) \langle \nu(\rho, t) \rangle = \int_1^{\rho^2} d(\rho'^2) \nu(\rho', t). \tag{14}$$

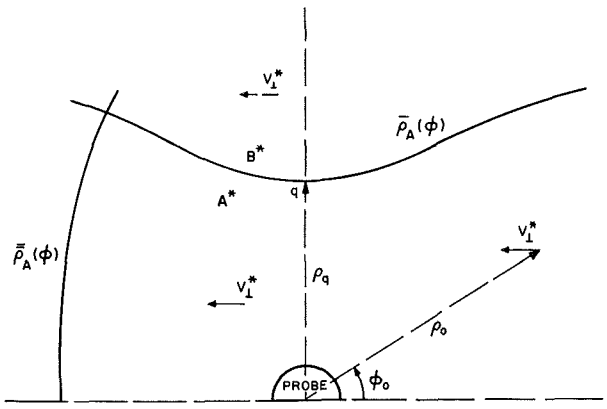

FIG. 2. Diagram showing regions A* and B* for simplest unperturbed ion distribution function in plane transverse to probe axis. A* is the set of the positions at $z=0$ (probe tip) of those ions that will strike the probe at some $z>0$.

$\delta(t)$ is found to change very little from $t=0$ to $t=\infty$ so that an intermediate constant value $\bar\delta$ can be used in Eq. (13); one finds

$$\bar\delta^{-1}=\ln\epsilon^{-1}+Y(\epsilon,\psi_p), \tag{15}$$

where Y is given in Fig. 1. $\langle\nu\rangle$ varies over the entire range $1\geq\langle\nu\rangle\geq 0$; however, in a certain neighborhood of the probe, roughly $\rho\lesssim\rho_m\equiv(2\psi_p\bar\delta)^{1/2}\epsilon^{-1}$, $\langle\nu\rangle$ is found to be always close to a central value $\bar\nu\equiv 0.80$. The error in the calculation of the current, resulting from these approximations, amounts to a few per cent.[6] Thus, for $\rho\gtrsim\rho_m$, the electric field may be correctly approximated by a function that only depends on ρ (conservative central field)

$$\frac{\partial\psi}{\partial\rho}=\frac{-\psi_p\bar\delta}{\rho}+\frac{\epsilon^2\bar\nu}{2\rho}(\rho^2-1). \tag{16}$$

Although for ϵ small the concept of a sheath has little meaning ("orbital motion limited" current implies an infinite sheath in the Langmuir sense[2]) both ρ_m and $\exp(\bar\delta^{-1})$, which are close to each other, may be thought of as characteristic sheath radii. If t_m is the typical time of flight to the probe of ions that were at the boundary of that sheath at $t=0$, it is clear that the theory is only valid for, roughly, $t\lesssim t_m$.

(ii) With the field known, ion trajectories may be computed explicitly. Moreover, the current to the probe is linear in the (unperturbed) ion distribution function at $t=0$, $f_0(\mathbf{v}_\perp^*)$. It suffices, therefore, to determine the current for the simplest possible f_0, that for which all ions have velocities of the same magnitude $v_\perp^*$ and direction (parallel to an arbitrarily chosen polar axis); see Fig. 2. Once that current $\bar\jmath^*(v_\perp^*)/j_\infty$ has been found, the current for any other f_0 is given by a definite integral, $\int f_0(\mathbf{v}_\perp^*)d\mathbf{v}_\perp^*\bar\jmath^*(v_\perp^*)/j_\infty$. To find $\bar\jmath^*/j_\infty$ one can use energy and angular momentum conservation to divide the (ρ,ϕ) plane at $t=0$ in two mutually exclusive regions $A^*(v_\perp^*)$ and $B^*(v_\perp^*)$: a point (ρ,ϕ) belongs to A^* if an ion having such initial coordinates, and moving under the field given by Eq. (16), strikes the probe at some $t>0$. The time of flight to the probe of every point in A^* can be computed and, therefore, a function $a^*(v_\perp^*,t)$ can be determined which represents the area of that part of A^* which has been "collected" by the time t. The current per unit length of probe is then

$$2\pi r_p j^*(t)=N_0 e\,da^*/dt \tag{17}$$

and defining $a(t)=\int a^* d\mathbf{v}_\perp^* f_0(\mathbf{v}_\perp^*)$, we have

$$2\pi r_p j(t)=N_0 e\,da/dt. \tag{18}$$

The average value of j is

$$\bar\jmath=(N_0 e/2\pi r_p)[a(t)/t] \tag{19}$$

and in nondimensional form

$$\bar\jmath/j_\infty=\epsilon\hat a(\tau)/(8\psi_p)^{1/2}\tau, \tag{20}$$

where $\tau=\omega_{pi}t$ and $\hat a$ is a nondimensional form of the area $\hat a=a/r_p^2$.

The general behavior of $\bar\jmath/j_\infty$ can be determined by a qualitative discussion of $\bar\jmath^*/j_\infty$ assuming that $v_\perp^*$ is of the order of the characteristic ion velocity. The condition for a point (ρ_0,ϕ_0) to belong to A^* follows from the equations of motion of an ion with initial coordinates (ρ_0,ϕ_0). One finds the condition

$$|\sin\phi_0|\leq G(\rho_0)/\rho_0, \tag{21}$$

$$G\equiv[1+\ln\rho_0^2/\alpha^*-\bar\nu(\rho_0^2-1)/\alpha^*\rho_m^2]^{1/2},$$

where

$$\alpha^*=2\beta^*/\psi_p\bar\delta,\qquad \beta^*=m_i(v_\perp^*)^2/2Z_i\kappa T_e. \tag{22}$$

For $\psi_p\gg 1$ and $\beta^*\leq 1$, as assumed here, we have $\alpha^*\ll 1$. For all $\alpha^*<1$ there is a value ρ_q such that $G(\rho_q)/\rho_q=1$ and then $G(\rho_0)/\rho_0>1$ for $\rho_0<\rho_q$; $\bar\rho_A(\phi)$, the boundary of A^* given by Eq. (21), has the form indicated in Fig. 2.[8] [As the ion temperature increases, α^* goes up and point q moves down reaching $\rho=1$ at $\alpha^*=1$; for $\alpha^*>1$, we have $G(\rho_0)/\rho_0\leq 1$ for all $\rho_0\geq 1$.] Now, $\partial\psi/\partial\rho\sim\rho^{-1}$ for, say, $\rho<\rho_m/3$ [see Eq. (16)] and the potential field is then logarithmic. The mean velocity of an ion with ρ_0 in that region, in its trip to the probe, is nearly independent of ρ_0; specifically, $\rho_0/\tau_0\sim\rho_m$, where $\tau_0(\rho_0,\phi_0)$ is the time of flight to the probe. Therefore, as long as $\rho_0<\rho_q$,

$$\hat a^*\sim\rho_m^2\tau^2\sim\psi_p\bar\delta\tau^2/\epsilon^2 \tag{23}$$

and

$$\bar\jmath^*/j_\infty\sim\epsilon\hat a^*/\tau\psi_p^{1/2}\sim\psi_p^{1/2}\tau\bar\delta/\epsilon. \tag{24}$$

$\bar\jmath^*/j_\infty$ grows linearly with τ until $\tau=\tau_q\equiv\tau_0(\rho_0=\rho_q,\ \phi_0=\frac{1}{2}\pi)$, when $\hat a^*$ switches from a quadratic growth in ρ_0 to a nearly linear one; for even larger τ, $\bar\jmath^*/j_\infty$ will actually decline because ions from outside the $\partial\psi/\partial\rho\sim\rho^{-1}$ region will begin to be collected and both field and ion mean velocity, ρ_0/τ_0, will rapidly decrease. Neglect-

ing logarithmic variations, from (21) we get

$$\rho_q \sim (\psi_p \bar{\delta}/\beta^*)^{1/2} \tag{25}$$

so that putting $\tau = \tau_q \sim \rho_q/\rho_m$ in (24) we obtain the peak in $\bar{\jmath}^*/j_\infty$:

$$\bar{\jmath}^*/j_\infty \sim (\psi_p/\beta^*)^{1/2}\bar{\delta}, \tag{26}$$

which can be far greater than unity and depends on β^*. The overshoot represented by (26) may be seen as caused by the sudden setup of the potential field which traps low angular momentum ions in the neighborhood of the probe; when β^* decreases, ρ_q increases and the low angular momentum region increases too. For decreasing ion temperature, a critical β^* is reached for which ρ_q moves out of the $\partial\psi/\partial\rho \sim \rho^{-1}$ region; the growth of $\bar{\jmath}^*/j_\infty$, as given in (24), is then stopped by the rapid decrease of ρ_0/τ_0, and not by the fact that the boundary of A^* has been reached. The effect is the same for all smaller β^* so that the current is now insensitive to that quantity. The critical value of β^* is found by putting $\rho_q \sim \rho_m$, i.e., $\tau_q \sim 1$,

$$\beta^* \sim \epsilon^2; \tag{27}$$

the maximum current peak possible is

$$\bar{\jmath}^*/j_\infty \sim \psi_p^{1/2}\bar{\delta}/\epsilon. \tag{28}$$

According to the Hester–Sonin similarity, the functions given in Eqs. (20) and (6) (for $\theta = 0$) are the same. Equation (20) depends on τ, ϵ, β, and ψ_p. In the flow problem the value corresponding to τ is $\tau_l \equiv \omega_{pi} t_l = \hat{l}/M$; the parameters $\hat{l}$ and M in Eq. (6) appear, therefore, combined in a single one. All the qualitative results derived above for $\bar{\jmath}/j_\infty$ need not be repeated and we shall only add two new points. (a) For the present problem, Eqs. (19) and (20) become

$$\bar{\jmath} = \frac{N_0 e U a(l/U)}{2\pi r_p l}, \tag{29}$$

$$\bar{\jmath}/j_\infty = [\epsilon M/(8\psi_p)^{1/2}\hat{l}]\hat{a}(\hat{l}/M). \tag{30}$$

Equation (29) makes clear the meaning of $a(l/U)$: The total current to the probe is

$$J = 2\pi r_p l \bar{\jmath} = N_0 e U a(l/U), \tag{31}$$

so that $a(l/U)$ is an effective probe cross section in the plane perpendicular to the flow. (b) As already indicated, the analysis of Ref. 6 is only valid for $t \lesssim t_m$; one finds that $\tau_m \equiv \omega_{pi} t_m \approx 3$. Thus, the results of the present paper will be valid for, roughly,

$$\hat{l} \lesssim 3M. \tag{32}$$

We note that the peak in $\bar{\jmath}/j_\infty$ occurs at $\tau \approx 1$.

The theory given above explains the large value of $\bar{\jmath}/j_\infty$ at $\theta = 0$. It can also explain its sharp decrease when the probe is turned by a small angle. For $\theta \neq 0$, the problem changes in three respects. First, the unperturbed distribution function in the (ρ, ϕ) plane, $f_0(\mathbf{v}_\perp^*)$, now has a drift velocity $U \sin\theta$; second, the Laplacian in Poisson's equation includes the term $\rho^{-2}\partial^2\psi/\partial\phi^2$; finally, angular momentum is not conserved. We shall now assume that the last two changes have no substantial effect on the current to the probe (this point is discussed in the appendix). Then, the results for $\bar{\jmath}^*(v_\perp^*)/j_\infty$, $v_\perp^*$ arbitrary, are not changed; the drift is taken into account by using the new form of $f_0(\mathbf{v}_\perp^*)$, which now has two characteristic velocities, $(\kappa T_i/m_i)^{1/2}$ and $U \sin\theta$. It is clear, therefore, that Eq. (6) may be written as

$$\bar{\jmath}/j_\infty = (\bar{\jmath}/j_\infty)[(\hat{l}/M\cos\theta), \epsilon, \beta, \tfrac{1}{2}(M^2\sin^2\theta), \psi_p]. \tag{33}$$

Now the characteristic values of β^* and α^* to be used in our earlier discussion on $\bar{\jmath}^*/j_\infty$ are not $\beta^* \sim \beta$ and $\alpha^* \sim 2\beta/\psi_p\bar{\delta}$ but, say,

$$\beta^* \approx \beta + \tfrac{1}{2}(M^2\sin^2\theta) \equiv \beta_T, \tag{34}$$

$$\alpha^* \approx (2/\psi_p\bar{\delta})[\beta + \tfrac{1}{2}(M^2\sin^2\theta)] \equiv \alpha_T \tag{35}$$

[although the effects of β and $M^2\sin^2\theta/2$ in (33) are not exactly additive, they may be considered so in a qualitative discussion]. As long as θ is so small that $\beta_T \approx \beta$, the current remains fairly constant. When θ becomes of the order of $(2\beta)^{1/2}/M$ or $(2\epsilon^2)^{1/2}/M$, whichever is the largest, the current begins to decrease. When θ is so large that $\alpha_T \geq 1$, we have $\rho_q \leq 1$ and so $G(\rho_0)/\rho_0$ in Eq. (21) is always less than one. Thus, $\hat{a}^*$ always grows (almost) linearly in ρ_0, while ρ_0/τ_0 remains fairly constant. Therefore, $\bar{\jmath}^*/j_\infty \approx 1$ (except for $\hat{l}/M\cos\theta$ very small). We note that, in fact, the peak in the current disappears for θ smaller than the value for which $\alpha_T = 1$.

Before using the results of the preceding time-dependent theory in the flow problem, we must examine the assumptions behind the Hester–Sonin similarity more carefully. First, if the $\partial^2\psi/\partial\zeta^2$ term is retained in Poisson's equation, Eq. (13) would read

$$\frac{\partial\psi}{\partial\rho} = \frac{-\psi_p\delta(\zeta)}{\rho} + \frac{\epsilon^2}{2\rho}\left\langle \nu(\rho,\zeta) - \hat{l}^{-2}\frac{\partial^2\psi}{\partial\zeta^2}\right\rangle(\rho^2-1), \tag{36}$$

where $\langle\ \rangle$ has the same meaning of Eq. (14) and we have used the variable ζ equivalent to τ. We want to find some quantitative condition for writing

$$\langle \nu - \hat{l}^{-2}\partial^2\psi/\partial\zeta^2\rangle \approx \langle\nu\rangle \tag{37}$$

in Eq. (36). The equation itself can be used to obtain $\partial^2\psi/\partial\zeta^2$ by integrating once with respect to ρ and differentiating twice with respect to ζ. If (37) is valid, we get

$$\hat{l}^{-2}\frac{\partial^2\psi}{\partial\zeta^2} = \frac{\psi_p\delta}{2\hat{l}^2}\left[2\delta\ln\rho\left\{\frac{d^2\delta^{-1}}{d\zeta^2} - 2\delta\left(\frac{d\delta^{-1}}{d\zeta}\right)^2\right\} + \frac{\bar{\delta}}{\delta}\int_1^\rho 2\frac{(\rho' - 1/\rho')d\rho'}{\rho_m{}^2}\left\langle\frac{\partial^2\nu}{\partial\zeta^2}\right\rangle\right]$$

so that

$$\left\langle \nu - \hat{l}^{-2}\frac{\partial^2\psi}{\partial\zeta^2}\right\rangle \approx \bar{\nu} - \frac{\psi_p\bar{\delta}}{2\hat{l}^2}\left[\bar{\delta}(2\ln\rho - 1)\right.$$

$$\left.\times\left\langle\frac{d^2\delta^{-1}}{d\zeta^2} - 2\bar{\delta}\left(\frac{d\delta^{-1}}{d\zeta}\right)^2\right\rangle + \frac{\rho^2}{2\rho_m{}^2}\left\langle\frac{\partial^2\nu}{\partial\zeta^2}\right\rangle\right].$$

Both $(2\ln\rho-1)$ and ρ^2 have maxima at the largest value of ρ considered; thus, we have

$$\left\langle \nu - \hat{l}^{-2}\frac{\partial^2\psi}{\partial\zeta^2}\right\rangle_{\rho\approx\rho_m} \approx \bar{\nu} - \frac{\psi_p\bar{\delta}}{2\hat{l}^2}$$

$$\times\left\langle 2\frac{d^2\delta^{-1}}{d\zeta^2} - 4\bar{\delta}\left(\frac{d\delta^{-1}}{d\zeta}\right)^2 + \frac{1}{2}\frac{\partial^2\nu}{d\zeta^2}\right\rangle.$$

We estimate $d\delta^{-1}/d\zeta \approx \Delta\delta^{-1}/\Delta\zeta < \delta^{-1}(\zeta=\infty)-\delta^{-1}(\zeta=0)$, $d^2\delta^{-1}/d\zeta^2 \approx 2\Delta\delta^{-1}$, $\partial^2\nu/\partial\zeta^2 \approx 2\Delta\nu$; for the typical values of ϵ and ψ_p to be considered later, $\delta^{-1}(\zeta=\infty)-\delta^{-1}(\zeta=0)\approx 0.15$ and $\Delta\nu < 0.20$.[6] Thus, we obtain

$$\left\langle \nu - \hat{l}^{-2}\frac{\partial^2\psi}{\partial\zeta^2}\right\rangle_{\rho\approx\rho_m} \approx \bar{\nu} - \frac{4\psi_p\bar{\delta}}{\hat{l}^2}\,0.1. \tag{38}$$

Since $4\bar{\delta}$ is never far from unity and the absolute error in writing $\langle\nu\rangle=\bar{\nu}$ is typically 0.1 [6] we find that the condition for the neglect of $\partial^2\psi/\partial\zeta^2$ in Poisson's equation is roughly

$$\hat{l} > \psi_p{}^{1/2}. \tag{39}$$

Second, if the z equation of motion of an ion is twice integrated up to $z=l$, with initial conditions $z=0$ and $dz/dt=U$, we get an equation for the time t_l that the ion takes to travel the probe

$$1 = (Ut_l/l)[1+(Ut_l/l)(\bar{\psi}_\zeta/2M^2)], \tag{40}$$

where $\bar{\psi}_\zeta$ is given by

$$t_l{}^2\bar{\psi}_\zeta = 2\int_0^{t_l}(t_l-t)\,dt\,\frac{\partial\psi}{\partial\zeta} \tag{41}$$

and this integral is along the trajectory of the ion. If $\partial\psi/\partial\zeta$ is small enough, the bracket in Eq. (40) becomes unity and we get the uniform motion assumption, $t_l=l/U$, on which the Hester–Sonin similarity is based. This can only be true if $\bar{\psi}_\zeta/2M^2$ is very small. Integrating Eq. (36) with respect to ρ and differentiating with respect to ζ we get

$$\frac{\partial\psi}{\partial\zeta} = \psi_p\ln\rho\,\delta^2\frac{d\delta^{-1}}{d\zeta} + \epsilon^2\int_1^\rho\frac{\rho'^2-1}{2\rho'}\,d\rho'\left\langle\frac{\partial\nu}{\partial\zeta}\right\rangle \tag{42}$$

so that, at most,

$$\bar{\psi}_\zeta/2M^2 \approx 0.4(\bar{\delta}\psi_p/4M^2), \tag{43}$$

where we considered the worst possible case (initial ρ equal to ρ_m) and estimated $d\delta^{-1}/d\zeta\approx 0.15$, $\partial\nu/\partial\zeta\approx 0.20$.

From Eq. (43) we conclude that if

$$\psi_p < M^2, \tag{44}$$

we have $t_l=l/U$ with an error of less than 3%.

Third, we note that 1) to actually obtain the current to the probe we must add the expression $N_0eU\pi r_p{}^2$ [the front end of the probe was excluded from $a(l/U)$] to Eq. (31), and 2) Sanmartin's analysis concerned a probe whose potential was switched from zero to V_p at $t=0$ (instead of a probe suddenly immersed in a plasma). The obvious corrections resulting from points 1) and 2) are only important if $\tau_l \ll 1$, but will be incorporated into the results in the next section.

III. THE ION CURRENT

The derivation of an expression for $\hat{a}^*$ (and thus for $\bar{\jmath}^*/j_\infty$ also) is detailed in the appendix of Ref. 6. The corrections indicated in the last paragraph above are equivalent to setting $\hat{a}_2{}^*=0$ in that appendix. Neglecting some small terms (that amount to less than 2% for ϵ, α^*, and $\psi_p{}^{-1}$ less than 0.1) we get (writing $\tau=\tau_l\equiv\hat{l}/M$)[9]

$$\bar{\jmath}^*/j_\infty = [\epsilon M/(8\psi_p)^{1/2}\hat{l}]\pi\sigma^2 \qquad \alpha^* < h, \tag{45}$$

$$= \frac{\epsilon M}{(8\psi_p)^{1/2}\hat{l}}\pi\sigma^2\left\{\frac{2}{\pi}\left[\sin^{-1}\left(\frac{h}{\alpha^*}\right)^{1/2} + \frac{(\alpha^*/h-1)^{1/2}}{\alpha^*/h}\right]\right.$$

$$\left. + \frac{h}{\alpha^*}2\,\frac{1-\sigma^{-2}}{\ln\sigma^2}\left[1 - \frac{2}{\pi}\sin^{-1}\left(\frac{h}{\alpha^*}\right)^{1/2} - \frac{2}{\pi}\left(\frac{\alpha^*}{h}-1\right)^{1/2}\right]\right\}$$

$$\alpha^* > h, \tag{46}$$

where σ is given by

$$\sigma\,\mathrm{erf}(\ln\sigma)^{1/2} = (2\psi_p\bar{\delta})^{1/2}\hat{l}/(\pi+0.6\hat{l}^2/M^2)^{1/2}M\epsilon \tag{47}$$

and

$$h = \ln\sigma^2/(\sigma^2-1). \tag{48}$$

The actual nondimensional ion current $\bar{\jmath}/j_\infty$ may be obtained from

$$\bar{\jmath}/j_\infty = \int d\mathbf{v}_\perp{}^* f_0(\mathbf{v}_\perp{}^*)(\bar{\jmath}^*/j_\infty). \tag{49}$$

The unperturbed ion distribution function in the plane $z=0$ is Maxwellian with a drift $U\sin\theta$ so that from Eq. (49) we get

$$\frac{\bar{\jmath}}{j_\infty} = \int_0^{2\pi}d\gamma\int_0^\infty v_\perp{}^* dv_\perp{}^*\,\frac{m_i}{2\pi\kappa T_i}$$

$$\times\exp\left\{\frac{-m_i}{2\kappa T_i}[(v_\perp{}^*)^2 + U^2\sin^2\theta\right.$$

$$\left.-2v_\perp{}^* U\sin\theta\cos\gamma]\right\}\bar{\jmath}^*/j_\infty$$

$$= \int_0^\infty\frac{dv}{\eta}\exp\left(-\frac{v}{\eta}\right)\exp\left(-\frac{\mu^2}{\eta}\right)I_0\left(2\frac{\mu}{\eta}v^{1/2}\right)\frac{\bar{\jmath}^*}{j_\infty}, \tag{50}$$

where I_0 is a modified Bessel function and

$$\eta=2\beta(\sigma^2-1)/\psi_p\bar{\delta}\ln\sigma^2, \qquad \mu^2=M^2\sin^2\theta(\sigma^2-1)/\psi_p\bar{\delta}\ln\sigma^2. \tag{51}$$

Using Eqs. (45) and (46) we can write (50) as

$$\bar{\jmath}/j_\infty=[\pi\epsilon\sigma^2M/(8\psi_p)^{1/2}\hat{l}]X(\mu,\eta,s), \tag{52}$$

where

$$X\equiv X_0(\mu,\eta)+sX_1(\mu,\eta), \qquad s=2(1-\sigma^{-2})/\ln\sigma^2, \tag{53}$$

and

$$X_0(\mu,\eta)\equiv X_0{}^{\mu\eta}=\eta^{-1}\exp\left(-\frac{\mu^2}{\eta}\right)\int_0^1 dv \times\exp\left(-\frac{v}{\eta}\right)I_0\left(\frac{2\mu v^{1/2}}{\eta}\right)+\eta^{-1}\exp\left(-\frac{\mu^2}{\eta}\right)\int_1^\infty dv \times\exp\left(-\frac{v}{\eta}\right)I_0\left(2\mu\frac{v^{1/2}}{\eta}\right)\frac{2}{\pi}\left[\sin^{-1}v^{-1/2}+\frac{(v-1)^{1/2}}{v}\right], \tag{54}$$

$$X_1(\mu,\eta)\equiv X_1{}^{\mu\eta}=\eta^{-1}\exp\left(-\frac{\mu^2}{\eta}\right)\int_1^\infty dv\exp\left(-\frac{v}{\eta}\right) \times I_0\left(\frac{2\mu v^{1/2}}{\eta}\right)v^{-1}\left[1-\frac{2}{\pi}\sin^{-1}v^{-1/2}-\frac{2}{\pi}(v-1)^{1/2}\right]. \tag{55}$$

It has not been possible to carry out the integrations in (54) and (55) analytically. A number of limiting expressions may easily be derived, however. For $\eta\to0$ (cold ion limit) we get

$$X_0{}^{\mu0}+sX_1{}^{\mu0}=1, \qquad \mu\leq1$$
$$=\frac{2}{\pi}\left[\sin^{-1}\mu^{-1}+\frac{(\mu^2-1)^{1/2}}{\mu^2}\right]$$
$$+\frac{s}{\mu^2}\left[1-\frac{2}{\pi}\sin^{-1}\mu^{-1}-\frac{2}{\pi}(\mu^2-1)^{1/2}\right] \qquad \mu\geq1. \tag{56}$$

For $\mu\to0$,

$$X_0{}^{0\eta}+sX_1{}^{0\eta}=\operatorname{erf}\eta^{-1/2}+2(\pi\eta)^{-1/2} \times\exp(-\eta^{-1})-2\eta^{-1}\operatorname{erfc}\eta^{-1/2}$$
$$+s[\eta^{-1}E_1(2\eta^{-1})-2(\pi\eta)^{-1/2}\exp(-\eta^{-1})\operatorname{erfc}\eta^{-1/2}]. \tag{57}$$

For η fixed and $\mu\to\infty$,

$$X_0{}^{\mu\eta}+sX_1{}^{\mu\eta}\approx X_0{}^{\mu0}+sX_1{}^{\mu0}\approx(4/\pi\mu)-s(2/\pi\mu); \tag{58}$$

all curves approach the cold ion limit. Finally, for μ^2/η fixed and $\eta\to\infty$

$$X_0{}^{\mu\eta}+sX_1{}^{\mu\eta}\approx[4/(\pi\eta)^{1/2}] \times\exp(-\mu^2/2\eta)I_0(\mu^2/2\eta)(1-\tfrac{1}{2}s); \tag{59}$$

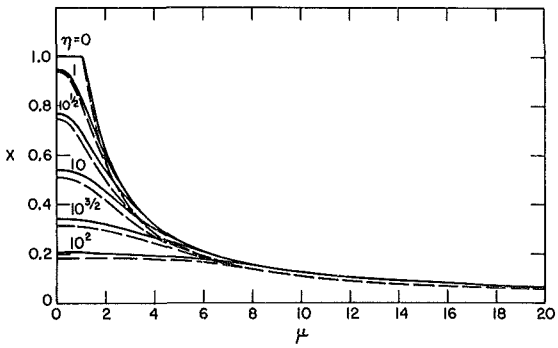

FIG. 3. Normalized current peak $X\equiv(2^{3/2}\psi_p{}^{1/2}\hat{l}/\pi\epsilon\sigma^2M)\bar{\jmath}/j_\infty$ versus normalized ion temperature $\eta\equiv2\beta(\sigma^2-1)/\psi_p\bar{\delta}\ln\sigma^2$, angle variable $\mu\equiv[(\sigma^2-1)/\psi_p\bar{\delta}\ln\sigma^2]^{1/2}M\sin\theta$, and parameter $s(\sigma)\equiv2(1-\sigma^{-2})/\ln\sigma^2$, full line $s=0$, dashed line $s=\frac{1}{3}$ (X is linear in s). $\bar{\delta}$ and σ (a normalized probe length) are defined in Eqs. (15) and (47); for other parameters, see first paragraph of Sec. II.

as $\mu^2/2\eta\to0$ this equation approaches $4(\pi\eta)^{-1/2}(1-\frac{1}{2}s)$, which is the limit of Eq. (57) as $\eta\to\infty$. Equation (59) can be also rewritten as

$$X_0{}^{\mu\eta}+sX_1{}^{\mu\eta}\approx(4/\pi\mu)(\mu^2/2\eta)^{1/2} \times\exp(-\mu^2/2\eta)I_0(\mu^2/2\eta)(2\pi)^{1/2}(1-\tfrac{1}{2}s); \tag{60}$$

as $\mu^2/2\eta\to\infty$, Eq. (60) approaches $4(1-\frac{1}{2}s)/\pi\mu$, which is the limit of Eq. (56) as $\mu\to\infty$.

$X\equiv X_0+sX_1$ is given graphically in Fig. 3 as a function of μ for several values of η. For each η, curves for two values of s have been represented ($s=0$, $s=\frac{1}{3}$); interpolation and extrapolation for different s are immediate because X is linear in s. We note that X is practically always very close to X_0. The function $X(\mu)$ is a direct representation of the peak structure, since $X\sim\bar{\jmath}/j_\infty$ and $\mu\sim\theta(\sin\theta\simeq\theta$ for the angles of interest).[10]

In the computation of X an overshoot was observed for the largest values of η in Fig. 3: in approaching the cold ions ($\eta=0$) curve, each (large) $\eta=$const curve overshot it and then approached it from above. This effect was so small that it did not show up clearly in the figure, and all curves were interrupted when first meeting the $\eta=0$ curve. The existence of the overshoot may be seen explicitly in Eq. (60), valid for large η, since the function

$$(2\pi y)^{1/2}\exp(-y)I_0(y),$$

which is zero at $y=0$ and unity at $y=\infty$, has a maximum 1.17, at $y\approx0.80$. Actually, this would indicate that the overshoot should be substantial; thus, one may conclude that for the moderately large values of η considered here, finite η effects partially mask the overshoot.

The fact that the $\eta=0$ curve is not an upper bound of the family $\eta=$const implies that the seemingly obvious condition $\partial X/\partial\eta<0$ is violated for some values of η and μ. That this is possible may easily be understood by noticing that if $\mathbf{v}_\perp{}^*$ is the vectorial composi-

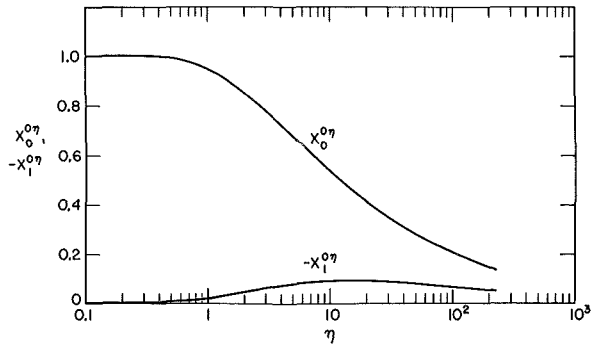

FIG. 4. Auxiliary functions $X_0{}^{0\eta}$ and $X_1{}^{0\eta}$ [see Eq. (57)] versus normalized ion temperature $\eta \equiv 2\beta(\sigma^2-1)/\psi_p\bar{\delta}\ln\sigma^2$. The maximum of the normalized current (occurring at $\theta=0$) is $X \equiv (2^{3/2}\psi_p{}^{1/2}\hat{l}/\pi\epsilon\sigma^2 M)\bar{\jmath}/j_\infty = X_0{}^{0\eta}+sX_1{}^{0\eta}$, where $s(\sigma)\equiv 2(1-\sigma^{-2})/\ln\sigma^2$. $\bar{\delta}$ and σ (a normalized probe length) are defined in Eqs. (15) and (47); for other parameters, see first paragraph of Sec. II.

tion of an equiprobably oriented (thermal) velocity and a directed velocity (the drift) forming an angle γ with each other, an increment of either component may decrease the value of $v_\perp{}^*$ for a certain range of values of γ; under some conditions the increase in current in this range may dominate the decrease that appears at all other values of γ.

From Eqs. (56) and (57), closed formulas may be derived for the main features of the current peak, that is, its maximum and its angular half-width $\hat{\theta}_{1/2}$ (the width of the peak at half-value of its maximum). For the maximum we have

$$\bar{\jmath}/j_\infty\,|_{\max} = (\bar{\jmath}/j_\infty)(\theta=0) = [\pi\epsilon\sigma^2 M/(8\psi_p)^{1/2}\hat{l}][X_0{}^{0\eta}+sX_1{}^{0\eta}]; \quad (61)$$

the functions $X_0{}^{0\eta}$ and $X_1{}^{0\eta}$, given in Eq. (57), are graphically represented in Fig. 4 for convenience. For the half-width we have the condition

$$X_0{}^{\mu\eta}+sX_1{}^{\mu\eta} = 0.5[X_0{}^{0\eta}+sX_1{}^{0\eta}], \quad (62)$$

where, from Eq. (52),

$$\mu = \hat{\mu}_{1/2} \equiv M\hat{\theta}_{1/2}(\sigma^2-1)^{1/2}/2(\psi_p\bar{\delta}\ln\sigma^2)^{1/2}. \quad (63)$$

We now note that all curves in Fig. 3 meet the cold-ion limiting curve at values of μ clearly smaller than $\hat{\mu}_{1/2}$. Thus, we can rewrite Eq. (62) as

$$X_0{}^{\mu 0}+sX_1{}^{\mu 0} = 0.5[X_0{}^{0\eta}+sX_1{}^{0\eta}]; \quad (64)$$

this equation only involves the functions given in Eqs. (56) and (57). A useful, explicit approximation for $\hat{\theta}_{1/2}$ may be obtained by neglecting the dependence on s and writing

$$X_0{}^{\mu 0} \approx 4/\pi[\mu^2+(4/\pi)^2-1]^{-1/2}$$

which has an error of less than 3%; we then have

$$\hat{\theta}_{1/2} \approx 2[\psi_p\bar{\delta}\ln\sigma^2/M^2(\sigma^2-1)]^{1/2} \times [(8/\pi X_0{}^{0\eta})^2+1-(4/\pi)^2]^{1/2}. \quad (65)$$

Equation (64) has been solved exactly for $s=0$ and $s=\frac{1}{3}$; $\hat{\mu}_{1/2}(\eta)$ is given graphically in Fig. 5.

Figure 6 presents $\bar{\jmath}/j_\infty\,|_{\max}$ versus $\hat{l}/M$ for a fixed ψ_p and several values of ϵ, from both Eq. (61) and the experimental data discussed in Ref. 5. Theoretical curves are presented for both $\beta=10^{-2}$ (solid line) and $\beta=10^{-3}$ (dashed line). In Ref. 5 it was estimated that in the experiments β was of order 10^{-2} or less, and it was assumed that a cold-ion theory would, therefore, apply. Our analysis shows that the condition for a cold-ion theory is not $\beta \ll 1$ but $\eta \ll 1$ (or more weakly, $\eta < 0.5$, say); this shows up clearly in Fig. 6 for the largest values of ϵ^{-1} and $\hat{l}/M$. The agreement with the experiments is excellent for $\epsilon=0.009$ and 0.041 if $\beta \approx 10^{-2}$; for $\epsilon=0.08$, the error is no more than 20% (except for a datum obviously in error), still within the error of the measurements. If β were 2×10^{-2}, say, the over-all agreement would improve greatly.

Hester and Sonin's experiments exhibited a linear dependence of the current on the potential; this is also in agreement with our theory since $j_\infty \sim \psi_p{}^{1/2}$ and $\bar{\jmath}/j_\infty \sim \psi_p{}^{1/2}$. On the other hand, Bettinger and Chen's theory predicted $\bar{\jmath} \sim \psi_p{}^{3/2}$.

Figure 7 presents a nondimensional half-width vs $\hat{l}/M$ for the same conditions of Fig. 6, from both theory (full line, $\beta=10^{-2}$, dashed line, $\beta=10^{-3}$) and experiments. The half-width $\theta_{1/2}$ is not $\hat{\theta}_{1/2}$; it is defined in the same way as $\hat{\theta}_{1/2}$, except that now the peak is defined as the current in excess of that predicted for an infinite probe. $[\theta_{1/2}]_{BC}$ is the prediction from the theory of Bettinger and Chen for cold ions. The use of $\theta_{1/2}$ allows direct comparison with the experiments of Ref. 5. The agreement is, in general, good for $\beta \approx 10^{-2}$.

The experiments showed no dependence of $\hat{\theta}_{1/2}$ (or of $\theta_{1/2}$) on ψ_p; this is also in complete agreement with our theory, as is easily verified in Eq. (65) (on the other hand, the theory of Ref. 3 predicted $\theta_{1/2} \sim \psi_p{}^{-1/4}$). We also note that for cold ions, our theory predicts that

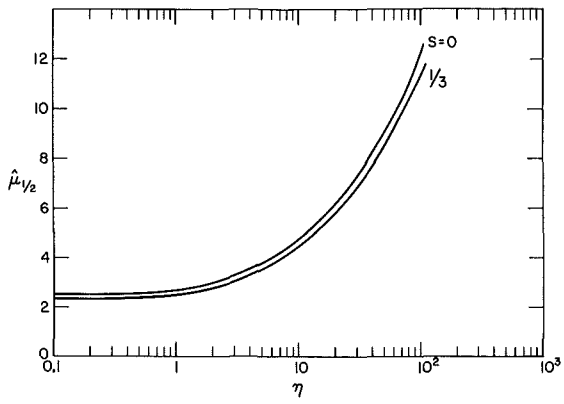

FIG. 5. Normalized angular half-width of current peak, $\hat{\mu}_{1/2} \equiv [(\sigma^2-1)/\psi_p\bar{\delta}\ln\sigma^2]^{1/2}M\hat{\theta}_{1/2}$ vs normalized ion temperature $\eta \equiv 2\beta(\sigma^2-1)/\psi_p\bar{\delta}\ln\sigma^2$ and parameter $s(\sigma) \equiv 2(1-\sigma^{-2})/\ln\sigma^2$. $\bar{\delta}$ and σ (a normalized probe length) are defined in Eqs. (15) and (47); for other parameters see first paragraph of Sec. II.

$\theta_{1/2}$ is linear in ϵ; this would explain the claim in Ref. 5 that the experimental data for $\theta_{1/2}/[\theta_{1/2}]_{BC}$ correlate in a single universal curve. However, we point out that for many of the experimental points of Fig. 7, as in Fig. 6, the ions cannot be considered as cold ($\eta>0.5$). (Even for cold ions, all curves do not exactly meet except for small $\hat{l}/M$, because of logarithmic effects.)

IV. CONCLUSIONS

The present paper deals with a significant end effect in the current response of a cylindrical Langmuir probe in a collisionless plasma flow. Infinitely-long-probe theory predicts that when the angle θ between probe axis and flow direction decreases, the current experiences a smooth decrease; for a finite probe, however, the current may exhibit a strikingly different behavior, in the form of a strong peak at small θ. The peak, which may be substantial even for very long probes, appears when the potential is highly negative and both the ion-acoustic Mach number M and the ratio of Debye length to probe radius ϵ^{-1} are large.

The only analyses of this end effect available until now were a rough theory for the regime $\hat{l}>3M$ ($\hat{l}$ being the ratio of probe length to Debye length)[3] and some numerical computations for $\hat{l}<3M$ and $\theta=0$.[5] Here, the regime $\hat{l}\lesssim 3M$ is rigorously studied for θ arbitrary within the peak region. The unperturbed ion distribution function is supposed to be Maxwellian. It is found that if $\bar{\jmath}$ is the current density at the probe surface, averaged over that surface, and $j_\infty \equiv \bar{\jmath}(\hat{l}\to\infty)$ [given in Eq. (7)], then $\bar{\jmath}/j_\infty$ may be written as

$$\bar{\jmath}/j_\infty = \bar{\jmath}/j_\infty(\hat{l}/M, \epsilon, \beta, \psi_p, M\theta), \qquad (66)$$

where β is the temperature ratio and $\psi_p=-eV_p/\kappa T_e$

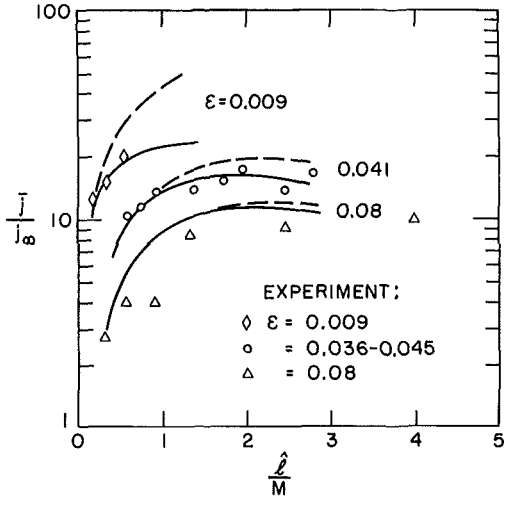

FIG. 6. Comparison of maximum nondimensional current density, $\bar{\jmath}/j_\infty(\theta=0)$, versus nondimensional probe radius ϵ and length $\hat{l}/M$, for $\psi_p=15$, from both experiments (Ref. 5) and present theory (full lines $\beta=10^{-2}$, dashed lines $\beta=10^{-3}$). All parameters are defined in first paragraph of Sec. II.

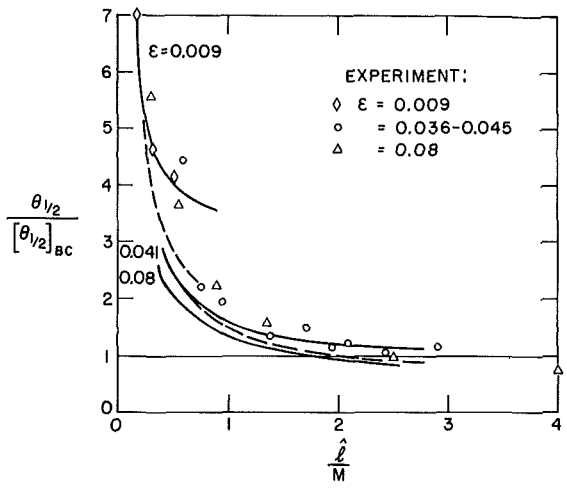

FIG. 7. Comparison of angular half-width (as defined in Ref. 5) from both experiments (Ref. 5) and present theory; same conditions of Fig. 6.

(V_p being the probe potential and T_e the electron temperature). Specifically, it is found that

$$[(8\psi_p)^{1/2}\hat{l}/\pi\epsilon M\sigma^2]\bar{\jmath}/j_\infty = X(\mu, \eta, s), \qquad (52')$$

where $\bar{\delta}$, σ, μ, η, and s are defined in Eqs. (15), (47), (51), and (53). The function $Y(\epsilon, \psi_p)$ in Eq. (15) is given in Fig. 1. In Eq. (51), $\sin\theta\simeq\theta$, since only narrow peaks are of interest.

An integral representation of the function X is given in Eqs. (53)–(55). Since X is linear in s, a single graph of the family of curves $X(\mu)$ with η as a parameter, for two values of s, covers all conditions; this graph is given in Fig. 3. This figure represents the peak structure $\bar{\jmath}/j_\infty(\theta)$, except for scaling factors, since $X\sim\bar{\jmath}/j_\infty$ and $\mu\sim\theta$. Explicit formulas for the main features of the peak (its maximum and its half-width) are presented in Eqs. (61), (64), and (56)–(57); these quantities can also be obtained graphically from Figs. 4 and 5. All predictions of the theory agree well with the experimental data (see Figs. 6 and 7).

The end effect may be advantageously used for diagnostic purposes. The first point to note is that the electron temperature has no effect on the peak: the dependence of $\bar{\jmath}/j_\infty$ on T_e cancels out except by way of $\bar{\delta}$; such dependence is very weak since the logarithmic variation in the term $\ln\epsilon^{-1}$ is substantially balanced by Y. Since j_∞ does not depend on T_e either, other aspects of probe response (usually the slope of the logarithm of the current for weakly negative potentials) must be used to determine T_e, if desired. The possibility of determining T_i without knowing T_e is itself an advantage.

Apart from parameters not related to the plasma (U, l, r_p) and a weak (logarithmic) functional dependency through $\bar{\delta}$ and $\ln\sigma$, the maximum and half-width

of the current peak can be written as

$$J_{\max}\sim -V_p F_1(N_0 Z_i/m_i,\ \kappa T_i/m_i), \tag{67}$$

$$\hat{\theta}_{1/2}\sim F_2(N_0 Z_i/m_i,\ \kappa T_i/m_i), \tag{68}$$

where F_1 and F_2 are known functions, N_0 is the plasma density and Z_i, m_i, T_i are the ion charge number, mass, and temperature. Since

$$J(\theta=\pi/2)\sim N_0(1-2Z_i eV_p/m_i U^2)^{1/2}, \tag{69}$$

$$J(\theta=\pi/2)/J(\theta=0,\ \hat{l}\to\infty)=(1-m_i U^2/2Z_i eV_p)^{1/2}, \tag{70}$$

it is possible to determine N_0, V_p, m_i/Z_i, and T_i/Z_i. The value $J(\theta=0,\ \hat{l}\to\infty)$ must be extrapolated from experimental data at moderately small θ; if such extrapolation is not accurate enough, an equation [Eq. (70)] is lost and some additional datum is required to find all four N_0, V_p, m_i/Z_i, T_i/Z_i. On the other hand, for cold enough ions, say $\eta<0.5$, we have $X\simeq X(\eta=0)$ and one of the unknowns is lost (T_i cannot be determined).

To the above-mentioned conditions on ϵ, ψ_p, $\cdots$ necessary for the presentation of the end effect, some additional conditions, due to the simplifications of the analysis, should be pointed out:

$$1\ll\hat{l}\lesssim 3M,$$

$$2\beta/\delta\ll\psi_p<M^2,\qquad \psi_p<\hat{l}^2.$$

ACKNOWLEDGMENTS

The author is very grateful to Professor A. A. Sonin for valuable discussions and suggestions.

This research was supported by the Advanced Research Projects Agency of the Department of Defense and was monitored by the Office of Naval Research under Contract No. N00014-0204-0040, ARPA Order No. 32.

APPENDIX

When the probe is not exactly aligned with the flow, the ion density is not centrally symmetric because of the drift $U\sin\theta$. In Sec. II it was assumed that this asymmetry had no visible effect on the ion current to the probe. The asymmetry shows up twice in the equation for the radial motion of an ion

$$\epsilon^2\frac{d^2\rho}{d\tau^2}=\frac{\partial\psi}{\partial\rho}+\frac{\epsilon^2}{\rho^3}\left[\lambda_0+\epsilon^{-2}\int_0^\tau\frac{\partial\psi}{\partial\phi}\,d\tau'\right]^2 \tag{A1}$$

where λ_0 is the nondimensional angular momentum at time $\tau\equiv\omega_{pi}t=0$ (when the ion crosses the $z=0$ plane) and the second term in the bracket represents the change in angular momentum due to the azimuthal field. When $\theta=0$, we have $\partial\psi/\partial\phi=0$ and it is possible to determine the region A^* and to find the function $\hat{a}^*(\tau)$ in Eq. (20) by using Eq. (16) in (A1). If $\theta\neq 0$, however, we have $\partial\psi/\partial\phi\neq 0$; $\partial\psi/\partial\rho$ now depends on ϕ, and the second term in the bracket in (A1) does not vanish.

To get an estimate of the importance of the asymmetry, we first note that in the plane $z=0$ the ion density is uniform. As z increases the ions readjust their distribution function. If the probe is sufficiently long, the "infinite" (two-dimensional) limit density is finally reached. For simplicity of discussion assume that the limit charge density can be written as

$$\nu_\infty=\nu_{c\infty}+\nu_{\phi\infty}\cos\phi, \tag{A2}$$

where $\nu_{c\infty}$ and $\nu_{\phi\infty}$ are functions of ρ only. A (very) conservative estimate of $\nu_{\phi\infty}$ for $\rho<\rho_m$ would be $\nu_{\phi\infty}=1$ [note that within the θ range of interest, the peak, we have $\alpha_T<1$ or $(M\sin\theta)^2/2\psi_p<\delta/2\ll 1$]; for $\rho>\rho_m$, we may take $\nu_{\phi\infty}=0$. If the probe is sufficiently short, the asymmetry has no time to develop. A conservative estimate of the time required to reach the limit charge density (A2) would be an ion plasma period or $\hat{l}=2\pi M$. The longest probes considered here have $\hat{l}\approx 3M$. Thus, we consider $\hat{l}\approx 3M$ and assume

$$\nu_\phi(z=0)=0,$$

$$\nu_\phi(z=l)=(3/2\pi)\nu_{\phi\infty}\cos\phi,$$

and a linear growth from $\nu_\phi(z=0)$ to $\nu_\phi(z=l)$. It is then possible to determine the ϕ-dependent part of ψ and its relative importance in Eq. (A1). We find that, under the worst conditions, the ϕ dependence affects no result by more than 10%. Because of the conservative conditions used, this should justify our neglecting $\partial\psi/\partial\phi$ in Sec. II.

There is an assumption underlying the preceding discussion and the main body of our analysis that deserves consideration. This assumption is that the ion distribution function at $z=0$ is the unperturbed distribution function far ahead of the probe. Obviously, the field ahead of the probe tip will somehow affect the ions reaching the plane $z=0$. Since $\epsilon\ll 1$ and the potential field around the tip should be roughly spherically symmetric, we can assume this field to be $\psi\approx\psi_p/\rho$, (in order to get a rough estimate of the importance of that effect). Then, the ion motion for $z<0$ can be solved exactly; we find, for instance, that

$$Z_i N_i/N_0(z=0)=1+[W^2/(1+2W)],$$

$$2W=(1+2\psi/M^2)^{1/2}-1.$$

It may be shown that the perturbations in ion density and ion azimuthal velocity are of no importance. The perturbation in ion radial velocity, however, may in some cases be so large as to affect the ion current to the probe. This occurs when the probe is very short ($\hat{l}\ll 3M$) and ψ_p/M^2 is close to unity [remember condition (44)].

Finally, since our entire analysis is restricted to the regime $\hat{l}\lesssim 3M$, we would like to comment briefly on

Bettinger and Chen's theory for the regime $\hat{l}>3M$.[3] To understand point (iv) below, we emphasize here that the limitation $\hat{l}\lesssim 3M$ of our analysis originates from our lack of a good approximation for $\partial\psi/\partial\rho$, for $\rho>\rho_m$; such values of ρ come into play when $\hat{l}>3M$. When $\partial\psi/\partial\rho$ is unknown, $\hat{a}^*(\tau)$, and thus $\bar{\jmath}/j_\infty$, cannot be determined.

In the light of our theory and of Fig. 2, Bettinger and Chen's approach may be summarized as follows: (i) they divided region A^* in two subregions, call them A_i and A_0, lying inside and outside the sheath, respectively. For the sheath radius [equivalent to our ρ_m or $\exp(\delta^{-1})$] they used an expression "a" patched up from numerical results for probes in quiescent plasmas. As pointed out in Ref. 5, "a" has a wrong dependence on ψ_p; this leads to the wrong dependence of $\bar{\jmath}$ and $\theta_{1/2}$ on ψ_p indicated in Sec. III. (ii) They assumed that all ions in A_i are collected; this leads to the requirement $\hat{l}>\tau_m M\approx 3M$. For A_0, they noticed that the appropriate equivalent time (probe length) was not $\tau_l\equiv\hat{l}/M$ but $\tau_l-\tau_m$. However, they did not incorporate this correction into their formulas; instead, in a comparison with some experiments, they appropriately adjusted the experimental data. This may lead to confusion: In the resume of Bettinger and Chen's theory given in Ref. 5, the correction was not considered; it may easily be verified that with such a correction the overall agreement in Figs. 5a, b, c of Ref. 5 would improve. (iii) To compute τ_m, power laws for $\partial\psi/\partial\rho$ were used instead of the correct expression given by our Eq. (16). The variation of τ_m with the particular power law is not greatly significant however. (iv) The most crucial point of their analysis is that for $\hat{a}^*$ inside A_0 they wrote

$$\hat{a}_0^*(\tau)\sim(\tau_l-\tau_m),$$

where the proportionality constant is obtained from the limit $\tau_l\to\infty$. This is obviously wrong because the value of ψ at the sheath boundary is still $O(1)$ so that for some distance outside the sheath, ion velocities are not well approximated by their asymptotic values, unless $\beta\gg 1$. (This point is related to the well-known Bohm's sheath criterion.) For $\beta\ll 1$ the error can be substantial except if τ_l is very large. (v) A final error is the approximation of $\bar{p}_A(\phi)$ everywhere by its asymptotic value. The approximation is good for A_0 but not for A_i. Thus, the resulting error should be noticeable for moderate τ_l.

Nevertheless, on the whole, the agreement of the theory of Ref. 3 with experiment is good for moderate potentials. Thus, it should be possible to use that theory for $\hat{l}>3M$, provided that an appropriate sheath radius (ρ_m) is used and the correction $\tau_l\to\tau_l-\tau_m$ is incorporated into the formulas.

* Present address: Instituto Nacional de Tecnica Aeroespacial, Madrid-1, Spain.

[1] J. G. Laframboise, University of Toronto Institute for Aerospace Studies Rept. No. 100 (1966).
[2] H. M. Mott-Smith and I. Langmuir, Phys. Rev. **28**, 727 (1926).
[3] R. T. Bettinger and A. A. Chen, J. Geophys. Res. **73**, 2513 (1968).
[4] S. D. Hester and A. A. Sonin, in *Rarefied Gas Dynamics* edited by L. Trilling and H. Wachman (Academic, New York, 1969), Vol. II, p. 1659.
[5] S. D. Hester and A. A. Sonin, Phys. Fluids **13**, 1265 (1970).
[6] J. R. Sanmartin, Phys. Fluids **15**, 391 (1972).

[7] $\bar{\jmath}(z)$ is the density current averaged over the contour of the probe at z.

[8] The second boundary of A^* in Fig. 2, $\bar{p}_A(\phi)$, excludes those ions below $\bar{p}_A(\phi)$ which initially move away from the probe ($\phi_0>\pi/2$) and never turn back. This boundary plays no role here because ions initially at that boundary have a time of flight to the probe larger than t_m.

[9] Equations (45) and (46) were not explicitly written in Ref. 6. Instead, the final result for $\bar{\jmath}/j_\infty$, after integrating $\bar{\jmath}^*/\bar{\jmath}_\infty$ over a Maxwelliam distribution, was presented in Eqs. (33)–(40) of that paper. The dominant terms given by (45) and (46) here, gave rise to X_1 in Ref. 6; X_2 and X_3 in that paper came from the small terms neglected here and from the component a_2^* of $\hat{a}^*$ mentioned above, respectively.

[10] The general trends in this and following diagrams are easily understood in the light of the discussion of Sec. II. The square corner in the peak for cold ions ($\eta=0$) in Fig. 3 occurs when $U\sin\theta$ is such that $\tau_l=\tau_q\equiv\tau_0(\rho_0=\rho_q,\ \phi_0=\pi/2)$. A finite ion temperature results in (1) a rounded corner because there is then a spectrum of values ρ_q, and (2) a decrease of $\bar{\jmath}/j_\infty(\theta=0)$.